

Supplement of Atmos. Chem. Phys., 16, 3743–3760, 2016  
<http://www.atmos-chem-phys.net/16/3743/2016/>  
doi:10.5194/acp-16-3743-2016-supplement  
© Author(s) 2016. CC Attribution 3.0 License.



Atmospheric  
Chemistry  
and Physics  
Open Access  
EGU

*Supplement of*

## **Mercury oxidation from bromine chemistry in the free troposphere over the southeastern US**

**Sean Coburn et al.**

*Correspondence to:* Rainer Volkamer ([rainer.volkamer@colorado.edu](mailto:rainer.volkamer@colorado.edu))

The copyright of individual parts of the supplement might differ from the CC-BY 3.0 licence.

## **S1 Instrument and Measurement Site**

The instrument and measurement site are identical to that described in Coburn et al. (2011). Only a brief overview will be given here. For the duration of the measurements discussed in this study, a research-grade MAX-DOAS instrument was located at a United States Environmental Protection Agency (US EPA) facility in Gulf Breeze, FL (30.3N 87.2W) and measured for time periods between May 2009 and February 2011. This site is ~10 km southeast of Pensacola, FL (population appr. 50,000) and ~1 km from the coast of the Gulf of Mexico, which enables the measurement of urban and marine air masses. The spectrometer and controlling electronics were set-up in the warehouse of the EPA facility, while the telescope was mounted on a support structure on the roof of the warehouse (~10-12 m above sea level) connected via an optical fiber. The telescope was oriented ~40° west of true north in order to realize a clear view in the lowest elevation angles to the coast. During operation the full 180° elevation angle range of the telescope was utilized to enable the characterization of air-masses over the seawater lagoon to the North, and over the coastal region of the Gulf of Mexico to the South. For the purposes of this study, the north viewing direction will be considered to minimize changes in the radiative transfer calculations due to azimuth effects throughout the day.

The instrument used for this study consists of a Princeton Instruments Acton SP2300i Czerny-Turner grating (500 groove/mm with a 300nm blaze angle) spectrometer with a PIXIS 400B back-illuminated CCD detector (Coburn et al., 2011). This setup was optimized to cover the wavelength range ~321-488 nm with an optical resolution of ~0.68 nm full-width at half the maximum (FWHM). The spectrometer is coupled to a weather-resistant telescope (capable of rotating the elevation angle by 180°, 50 mm f/4 optics) via a 10 m long 1.7 mm diameter quartz fiber. During normal field operation this instrument was routinely able to realize values of the root mean square (RMS) of the residual remaining after the DOAS fitting procedure on the order  $0.9-3 \times 10^{-4}$ . This system was very stable, with little need for maintenance, and was operated remotely for periods between May 2009 and February 2011 to measure multiple trace gases, including: BrO, IO, nitrogen dioxide (NO<sub>2</sub>), formaldehyde (HCHO), glyoxal (CHOCHO), and the oxygen molecule collision induced absorption signal (referred to as O<sub>4</sub>).

## **S2 DOAS retrieval sensitivity studies**

**S2.1 Retrieval window:** Several sensitivity studies were performed to determine the most suitable analysis settings for the BrO retrieval. This was accomplished through a comparison of both O<sub>3</sub> and HCHO dSCD values from the BrO fitting window with dSCDs predicted using WACCM vertical profiles. Also, the effect of using different O<sub>4</sub> reference cross-sections was tested with respect to the O<sub>4</sub> dSCD in the BrO fitting window.

WACCM model output profiles for O<sub>3</sub> and HCHO were used to forward calculate dSCDs for comparison to measured dSCDs of O<sub>3</sub> and HCHO retrieved using the BrO fitting window. Five different BrO analysis setting windows were tested: 1) fitting window 345-359nm with a 2<sup>nd</sup> order polynomial (encompasses two BrO absorption peaks – 2-band analysis); 2) fitting window 346-359nm with a 2<sup>nd</sup> order polynomial (2-band analysis); 3) fitting window 340-359nm with a 3<sup>rd</sup> order polynomial (3-band analysis); 4) fitting window 340-359nm with a 5<sup>th</sup> order polynomial (3-band analysis); and 5) fitting window 338-359nm with a 5<sup>th</sup> order polynomial (4-band analysis). It was determined that analysis setting 5) (4-band analysis with 5<sup>th</sup> order polynomial) including a constrained intensity offset (Sect. S2.2) best represented both O<sub>3</sub> and HCHO. These are the analysis settings that were then used to assess the effects of different O<sub>4</sub> cross sections in the BrO fitting window: 1) Hermans (2002); 2) Greenblatt et al. (1990); and 3) Thalman and Volkamer (2013). The O<sub>4</sub> dSCDs retrieved from the BrO fitting window were compared with the O<sub>4</sub> dSCDs retrieved from an O<sub>4</sub> optimized fitting window in the UV (353-387 nm); and while none of the cross sections are able to fully reproduce the O<sub>4</sub> dSCDs from the O<sub>4</sub> optimized window, the Thalman and Volkamer (2013) cross-section was deemed to be an improvement over Hermans and Greenblatt/Burkholder in representing O<sub>4</sub> in the BrO fitting window.

**S2.2 Intensity offset:** An additional parameter that can be utilized in the DOAS retrieval is an intensity offset, which would be used to help account for any instrument stray light. The instrument employed for this study was designed to actively minimize spectrometer stray light through the use of cut-off filters (BG3 and BG38), as well as the method of background correction. The background correction is similar to that described in Wagner et al. (2004) and utilizes dark regions on the CCD detector to correct for dark current and offset noise as well as stray light. It was determined that stray light in the instrument was only a few percent (before

correction) in the wavelength range 330-360 nm. Fitting an intensity offset should only account for uncorrected stray light and is expected to be on the order of magnitude of the error in the background correction. The fitting of this parameter typically helps reduce the RMS of the fitting routine, thus improving instrument sensitivity. However, preliminary studies found a significant effect on the retrieved BrO dSCDs depending on whether or not this parameter was included in the fitting routine, and that this effect was most pronounced in the narrower fitting windows. In the most extreme case (analysis window 346-359 nm), retrieved BrO dSCDs changed from  $\sim 1 \times 10^{14}$  molec cm<sup>-2</sup> without fitting the intensity offset to values less than zero when an unconstrained intensity offset was included. In all fitting windows tested, utilizing an unconstrained intensity offset resulted in the highest fit factor for the offset and lowest values for the BrO dSCDs, and in some cases lead to significantly negative (non-physical) values. In these cases, it was found that periods of time existed when the fit factor for the intensity offset was much greater than what was determined to be a reasonable value for this instrument. For this reason, the intensity offset was kept in the retrieval (to help with RMS), but limited to a range determined by the upper limit of this estimated correction ( $\pm 3 \times 10^{-3}$ ).

Based on the findings of the offset sensitivity tests and the dSCD comparison tests presented in this section, the dSCDs used for the BrO inversion are from the 338-359 nm fitting window utilizing a 5<sup>th</sup> order polynomial, the constrained intensity offset, and the Thalman and Volkamer (2013) O<sub>4</sub> cross-section.

### **S3 Aerosol Retrieval**

Aerosol profiles are determined through an iterative comparison of measured O<sub>4</sub> dSCDs (analyzed in the wavelength window 437-486 nm) with O<sub>4</sub> dSCDs calculated from the RTM McArtim3 (Deutschmann et al., 2011) outputs based on specific aerosol extinction profiles. This process is performed on each set of MAX-DOAS viewing angles (for this point forward referred to as a scan) of the case study day (total of 56 scans) in order to determine individual aerosol profiles. The initial aerosol profile used for each scan decreased exponentially with altitude from a value of 0.01 km<sup>-1</sup> at 483 nm (scale height of 0.6 km). This wavelength is chosen for its proximity to the O<sub>4</sub> peak absorption structure at 477 nm while avoiding the feature itself, as well as avoiding absorption structures from other trace gases (i.e. NO<sub>2</sub>). This O<sub>4</sub> fitting window was chosen due to

the better general agreement achieved between measured and forward calculated  $O_4$  dSCDs (calculated after aerosol extinction profiles were determined) as compared with the  $O_4$  retrieval in the UV range. This is similar to findings from Volkamer et al., (2015), where it is determined that using the 477 nm  $O_4$  band for deriving aerosol profiles is much more robust than using the UV bands due to the increased Rayleigh scattering at shorter wavelengths, which can mask aerosol extinction.

The  $O_4$  vertical profiles used for all calculations and as input to the RTM are based on temperature and pressure profiles available from NOAA's ESRL Radiosonde Database for locations close to the measurement site, which are in good agreement with the corresponding profiles from WACCM. In each step of the iteration the measured  $O_4$  dSCDs are compared to the forward calculated dSCDs at each elevation angle of the scan being analyzed, and the differences between these values are used as input for optimizing the modification of the aerosol profile for the subsequent iteration. For this study, the convergence limit is set at a percent difference of 5% between the lowest two elevation angle dSCDs, or if the process reaches 5 iterations without finding convergence the last aerosol profile is used. The limit of 5 iterations is chosen as a compromise between achieving optimal agreement between the  $O_4$  dSCDs and data computation time. For this case study, the 5% criterion is reached for every sequence. The resulting time series of aerosol extinction profiles are shown in Fig. S10 (Supplement).

The aerosol extinction profiles at 483 nm were scaled to derive extinction at 350 nm using the relationship found in Eq. (S1).

$$\epsilon_{350} = \epsilon_{483} \cdot \left(\frac{350}{483}\right)^{-1.25} \quad (S1)$$

where  $\epsilon_{350}$  and  $\epsilon_{483}$  represent aerosol extinction coefficients at 350 and 483 nm, respectively. An Angstrom exponent of -1.25 was chosen as a moderate value that would be representative of an average atmosphere (Dubovik et al., 2002). The retrieved aerosol profiles at 350 nm provided input to the RTM in order to calculate the appropriate weighting functions for BrO.

#### **S4 Box Model Description**

The modeling portion of this study is designed to assess the concentration of Br radicals available to participate in the mercury oxidation reaction based on BrO vertical profiles provided from the MAX-DOAS measurements and GEOS-Chem. Other trace gas and atmospheric parameter inputs

to the diurnal steady-state box model (Dix et al., 2013, Wang et al., 2015) are median daily profiles derived from the MAX-DOAS measurements, WACCM, and GEOS-Chem. A single median profile representing the entire day (daily median, for each model input) is used rather than individual profiles. From these profiles, the box model then calculates the partitioning between bromine species throughout the troposphere (including: reactions with other trace gases; photolysis; and some aqueous phase partitioning and chemistry) in order to derive vertical profiles of the Br radical, which are subsequently used for calculating mercury oxidation rates. A summary of all the reactions involving mercury compounds considered in the box model along with associated rate coefficients can be found in Table 2. The model conceptually follows the framework of Crawford et al., (1999), where model inputs are initiated and allowed to reach steady-state over several days. In the box model, the BrO and IO (to assess the impact of iodine radical species in the mercury oxidation reactions) profiles are taken from the MAX-DOAS measurements; however, the GEOS-Chem BrO profile is also used in order to assess the impact of the differences between these profiles. Other box model inputs are taken as the output profiles from the external models utilized in this study and these include: temperature, pressure, and HCHO from WACCM; and O<sub>3</sub> and NO<sub>2</sub> from GEOS-Chem. As a sensitivity test WACCM O<sub>3</sub> and NO<sub>2</sub> were also used to assess the impact on the mercury oxidation scheme towards differences in the vertical distributions of these molecules. The resulting vertical profiles of the rate of mercury oxidation using these two profiles as box model inputs is found in Fig. S11 (Supplement), which follows the same format as Fig. 7. Aerosol surface area measurements from the TORERO data set (Volkamer et al., 2015; Wang et al., 2015) are assumed representative of conditions in the marine atmosphere, and therefore used as model inputs for lack of independent measurements. The vertical distribution of Hg<sup>0</sup> from GEOS-Chem was used in all scenarios. Additionally, photolysis rates for a variety of species, calculated using the Tropospheric Ultraviolet and Visible (TUV) Radiation model, are included. The TUV model was initiated for a Rayleigh atmosphere (aerosol extinction = 0), with O<sub>3</sub> and NO<sub>2</sub> columns of 380 and 0.3 Dobson Units (DU), respectively, which are derived from the average vertical profiles from WACCM. Since the median BrO profile derived by the MAX-DOAS measurements closely resembles the profiles retrieved around solar noon (see Fig. 5), the TUV calculations from this time are used. For the

model runs comparing the BrO profiles from the measurements and GEOS-Chem, only the BrO profile is changed; all other inputs remain constant.

For the determination of the dominant oxidative pathways, the reaction rates for oxidation of  $\text{Hg}^0$  against Br and  $\text{O}_3$  are calculated as a function of altitude for the different reactant vertical profiles, which is important due to atmospheric temperature gradients. This also allows the assessment of the relative contributions of these reactions to the overall rate of oxidation as a function of altitude. Oxidation by  $\text{O}_3$  is included in the box model due to the amount of evidence from laboratory studies indicating that this reaction might play a role in the atmosphere; although potentially not completely in the gas phase.

Following Wang et al. (2015), the box model is initiated under two different modes to investigate the sensitivity of oxidation rates, and likely product distributions to the mechanistic assumptions about mercury oxidation. The two modes differ in the scavenging reactions of the HgBr adduct. A “traditional” scenario only includes Br and OH radicals as scavengers (Holmes et al., 2009), and a “revised” mode includes species suggested by Dibble et al., 2012 (BrO,  $\text{NO}_2$ , and  $\text{HO}_2$ ) as well as additional halogen species (I and IO). The model also tracks the concentrations of all species as a function of altitude, which gives indications for the product distributions of the various reactions.

## References (Supplement)

- Coburn, S., Dix, B., Sinreich, R., and Volkamer, R.: The CU ground MAX-DOAS instrument: characterization of RMS noise limitations and first measurements near Pensacola, FL of BrO, IO, and CHOCHO, *Atmos. Meas. Tech.*, 4, 2421-2439, 10.5194/amt-4-2421-2011, 2011.
- Crawford, J., Davis, D., Olson, J., Chen, G., Liu, S., Gregory, G., Barrick, J., Sachse, G., Sandholm, S., Heikes, B., Singh, H., and Blake, D.: Assessment of upper tropospheric HOx sources over the tropical Pacific based on NASA GTE/PEM data: Net effect on HOx and other photochemical parameters, *J. Geophys. Res. -Atmos.*, 104, 16255-16273, 10.1029/1999JD900106, 1999.
- Deutschmann, T., Beirle, S., Friess, U., Grzegorski, M., Kern, C., Kritten, L., Platt, U., Prados-Roman, C., Pukite, J., Wagner, T., Werner, B., and Pfeilsticker, K.: The Monte Carlo atmospheric radiative transfer model McArtim: Introduction and validation of Jacobians and 3D features, *J. Quant. Spectrosc. Radiat. Transfer*, 112, 1119-1137, 10.1016/j.jqsrt.2010.12.009, 2011.
- Dibble, T. S., Zelig, M. J., and Mao, H.: Thermodynamics of reactions of ClHg and BrHg radicals with atmospherically abundant free radicals, *Atmos. Chem. Phys.*, 12, 10271-10279, 10.5194/acp-12-10271-2012, 2012.
- Dix, B., Baidar, S., Bresch, J. F., Hall, S. R., Schmidt, K. S., Wang, S., and Volkamer, R.: Detection of iodine monoxide in the tropical free troposphere, *Proc. Natl. Acad. Sci. U. S. A.*, 110, 2035-2040, 10.1073/pnas.1212386110, 2013.
- Dubovik, O., Holben, B., Eck, T.F., Smirnov, A., Kaufman, Y.J., King, M.D., Tanre, D., Slutsker, I.: Variability of absorption and optical properties of key aerosol types observed in worldwide locations, *J. Atmos. Sci.*, 59, 3, 590-608, doi: 10.1175/1520-0469(2002)059<0590:VOAOP>2.0.CO;2, 2002.
- Greenblatt, G., Orlando, J., Burkholder, J. and Ravishankara, A.: Absorption-Measurements of Oxygen between 330nm and 1140nm, *J. Geophys. Res. -Atmos.*, 95, 18577-18582, 10.1029/JD095iD11p18577, 1990.

- Hermans, C., Measurement of absorption cross sections and spectroscopic molecular parameters: O<sub>2</sub> and its collisional induced absorption:  
<http://www.aeronomie.be/spectrolab/o2>, 2002.
- Wagner, T., Dix, B., von Friedeburg, C., Frieß, U., Sanghavi, S., Sinreich, R., and Platt, U.: MAX-DOAS O<sub>4</sub> measurements: A new technique to derive information on atmospheric aerosols. Principles and information content, *J. Geophys. Res.* 109, D22205, doi:10.1029/2004JD004904, 2004.al. (2004)
- Holmes, C. D., Jacob, D. J., Mason, R. P., and Jaffe, D. A.: Sources and deposition of reactive gaseous mercury in the marine atmosphere, *Atmos. Environ.*, 43, 2278-2285, 10.1016/j.atmosenv.2009.01.051, 2009.
- Thalman, R. and Volkamer, R.: Temperature dependent absorption cross-sections of O<sub>2</sub>-O<sub>2</sub> collision pairs between 340 and 630 nm and at atmospherically relevant pressure, *Phys. Chem. Chem. Phys.*, 15, 15371-15381, 10.1039/c3cp50968k, 2013.
- Volkamer, R., Baidar, S., Campos, T. L., Coburn, S., DiGangi, J. P., Dix, B., Eloranta, E., Koenig, T. K., Morley, B., Ortega, I., Pierce, B. R., Reeves, M., Sinreich, R., Wang, S., Zondlo, M. A., and Romashkin, P. A.: Aircraft measurements of BrO, IO, glyoxal, NO<sub>2</sub>, H<sub>2</sub>O, O<sub>2</sub>-O<sub>2</sub> and aerosol extinction profiles in the tropics: Comparison with aircraft-/ship-based in situ and lidar measurements, *Atmos. Meas. Tech.* 8, 2121-2148, 2015. doi:10.5194/amt-8-2121-2015.
- Wang, S., Schmidt, J.A., Baidar, S., Coburn, S., Dix, B., Koenig, T., Apel, E.C., Bowdalo, D., Campos, T.L., Eloranta, E., Evans, M.J., diGangi, J.P., Zondlo, M.A., Gao, R.S., Haggerty, J.A., Hall, S.R., Hornbrook, R.S., Jacob, D.J., Morley, B., Pierce, B.R., Reeves, M., Romashkin, P.A., ter Schure, A., and Volkamer, R.: Active and widespread halogen chemistry in the tropical and subtropical free troposphere, *P. Natl. Acad. Sci. USA*, 2015.

## Figure Captions

**Figure S1:** BrO box-AMFs for two elevation angles (25° and 90°, solid and dashed lines respectively) at different SZAs. For these higher pointing elevation angles, the box-AMFs peak at altitudes of 2-15km (free troposphere) for SZAs lower than 70°, while at higher SZA the box-AMFs indicate that the sensitivity towards the free troposphere is decreasing.

**Figure S2:** Overview of box-AMFs for SZAs less than 70° for 4 elevation angles: a) 3.8°; b) 10°; c) 25°; and d) 90°.

**Figure S3:** Overview of the WACCM BrO vertical profiles as a function of altitude and time of day (panel a), and then collapsed into to the corresponding partial (green trace) and total (blue trace) VCDs in panel b.

**Figure S4:** Example results for the inversion of IO from the MAX-DOAS measurements. Panel a) contains the three a-priori profiles used in the inversion (dashed, colored lines), the a-posteriori results from a MAX-DOAS scan at ~45° SZA (morning) corresponding to the a-priori profiles (solid lines, colors correspond with the a-priori), and the median IO profile (red trace, where the error bars reflect the 25<sup>th</sup> and 75<sup>th</sup> percentiles). Panel b) shows the averaging kernels for the inversion using a-priori “Prf1”. Panel c) shows the diurnal variation of the IO VCD for the BL (0-1 km), troposphere (0-15 km), and total (0-25 km).

**Figure S5:** Overview of the sensitivity of  $SCD_{Ref}$  and the derived VCDs on the choice of reference spectra/scan and a-priori profile assumption. Panel (a) contains the  $SCD_{Ref}$  determined from both forward calculations of the a-priori profiles (grey traces) and the iterative approach (blue traces) for 47 different zenith spectra. The a-priori cases corresponding to the median BrO profile based on WACCM (WACCM\*1.4) are denoted with thicker and darker lines. The error bars on the forward calculated median BrO profile case (dark grey) reflect the  $\pm 1 \times 10^{13}$  molec cm<sup>-2</sup> criteria for selecting suitable references. Panel (b) contains the corresponding VCDs derived for one MAX-DOAS scan (near solar noon) for each of the references and a-priori combinations. The blue shaded vertical boxes denote references that meet the criteria for being used in the inversion; and the horizontal grey box (panel b) covers the range of  $2.3 \pm 0.9 \times 10^{13}$  molec cm<sup>-2</sup>, which fully captures all the references contained within the shaded blue region.

**Figure S6:** Time series of the DoFs and inversion RMS for three different analysis procedures: 1) changing reference analysis (reference is selected from each measurement scan throughout the day, blue trace); 2) fixed reference without accounting for any  $SCD_{Ref}$  (green trace); and 3) fixed reference analysis accounting for  $SCD_{Ref}$  (red trace). Included in the plot is SZA (black trace) for reference.

**Figure S7:** Shows a comparison of the measured BrO dSCDs and the dSCDs calculated from the a-posteriori profiles (inversion using the WACCM profile) for both the entire case study day (panel a) and for a small subset of scans before solar noon (panel b). Panel c contains the RMS of the difference between the measured and calculated dSCDs for each scan.

**Figure S8:** Overview of vertical profiles of parameters used as input to the box model utilized in this study which were: 1) from WACCM (temperature, pressure, HCHO); 2) from GEOS-Chem (BrO,  $O_3$ ,  $NO_2$ , and  $Hg^0$ ); 3) from the TORERO field experiment (total surface area); and 4) derived during this study (BrO and IO).

**Figure S9:** Observed concentrations of selected trace gases during April 2010 at the Pensacola MDN site. Note scale factors for some species given in the legend.

**Figure S10:** Comparison of measured  $O_4$  dSCDs and dSCD calculated based on the derived aerosol profiles for the entire case study day (panel a) and a subset of scans (panel b). Panel c contains the diurnal variation in the derived aerosol profiles, and an example profile is found in panel d.

**Figure S11:** Box model results of the rate of mercury oxidation as a function of altitude for two species: 1) ozone (red); and 3) bromine radicals (solid blue: MAX-DOAS; dashed pink: GEOS-Chem) (panel a); the corresponding lifetimes are found in panel b. The black dashed line at 4 km shows where measurement sensitivity starts to drop because of the decreasing amount of BrO (the measured parameter) in the lower layers of the atmosphere. This figure is complementary to Fig. 7, but uses the WACCM, rather than GEOS-Chem,  $O_3$  and  $NO_2$  vertical profiles as input.

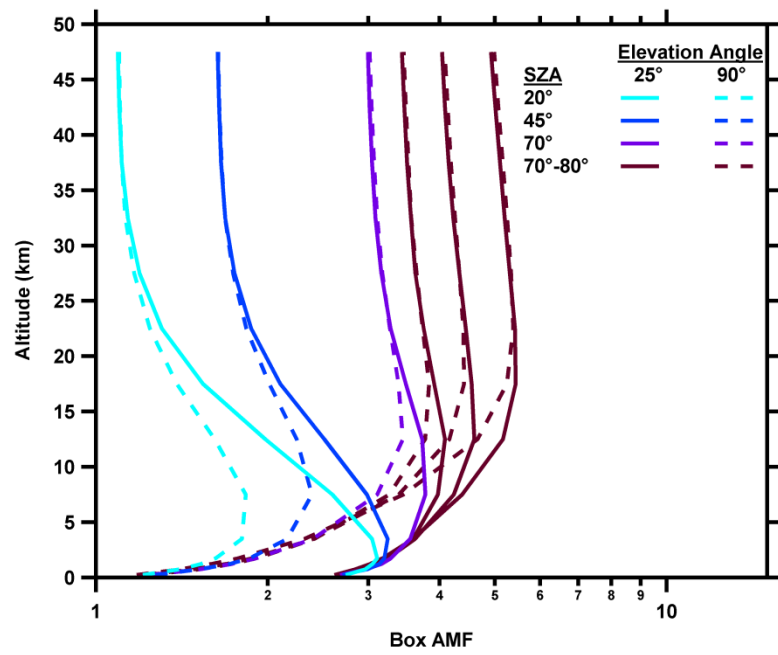


Figure S1

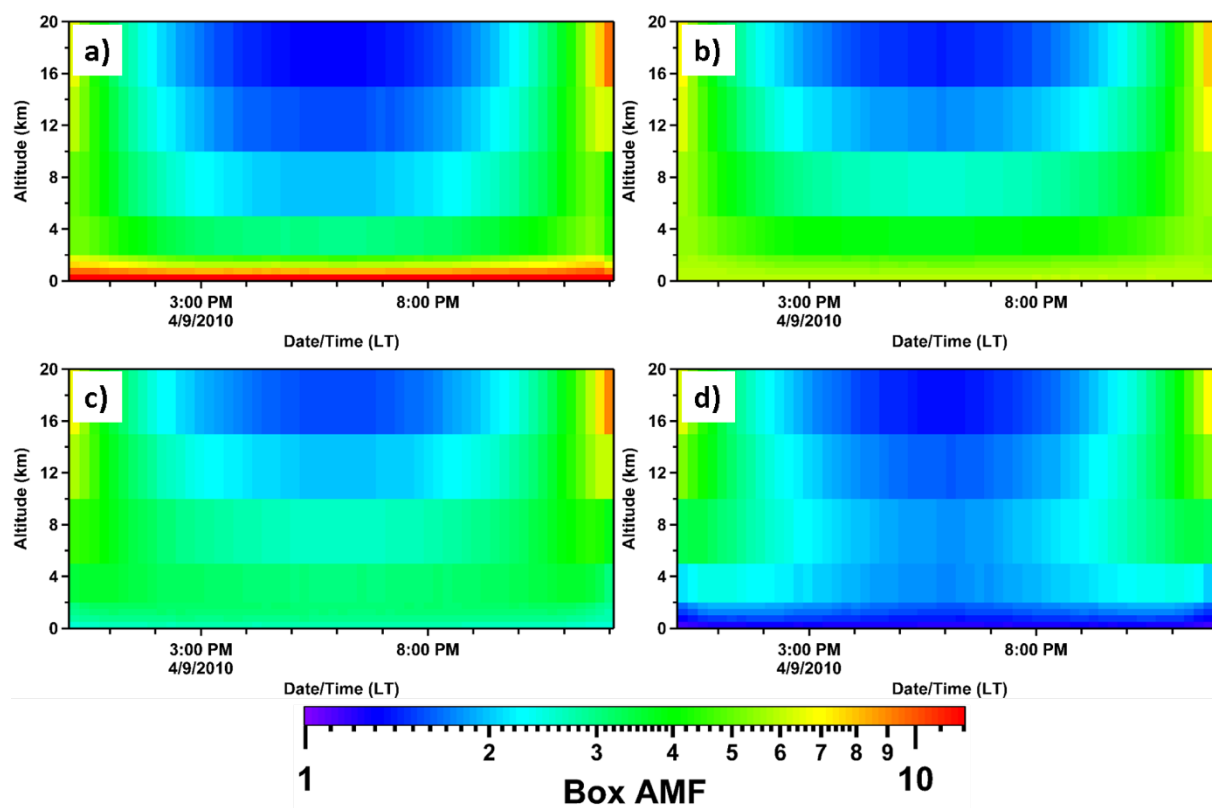


Figure S2

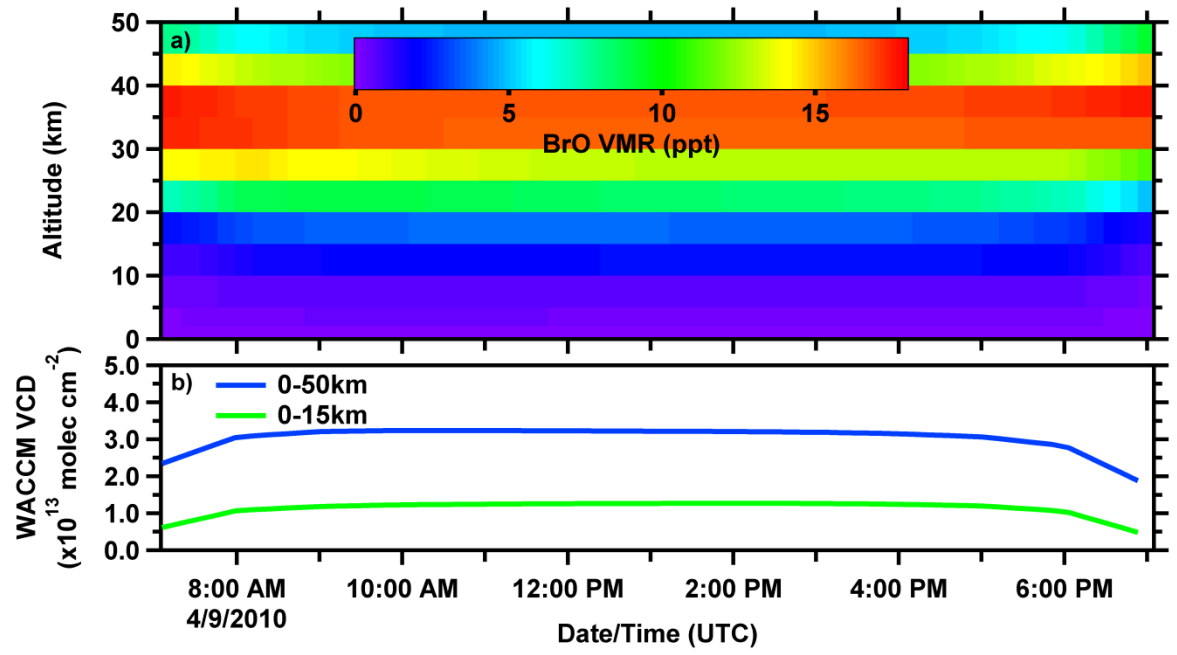


Figure S3

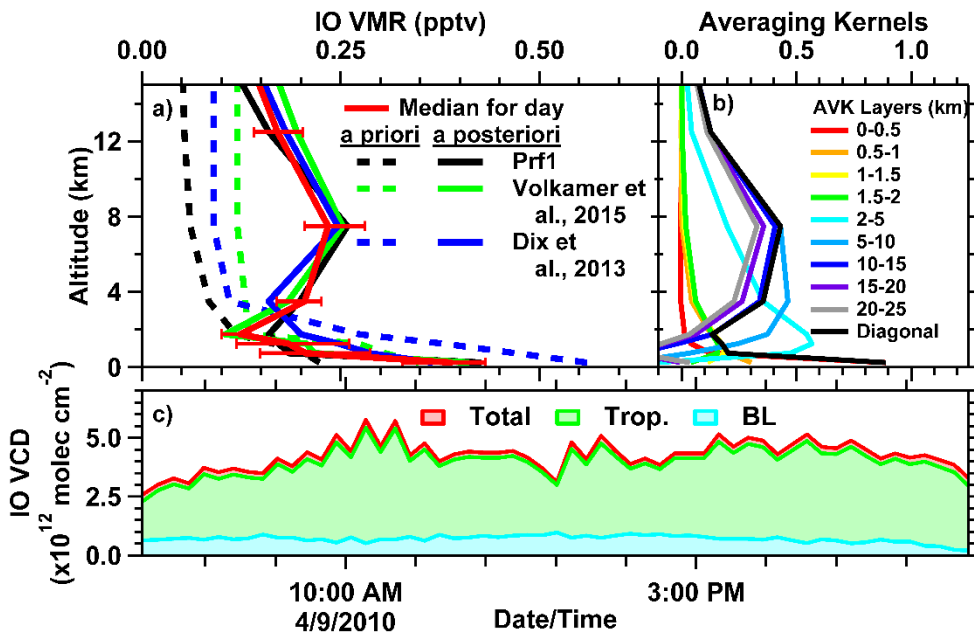


Figure S4

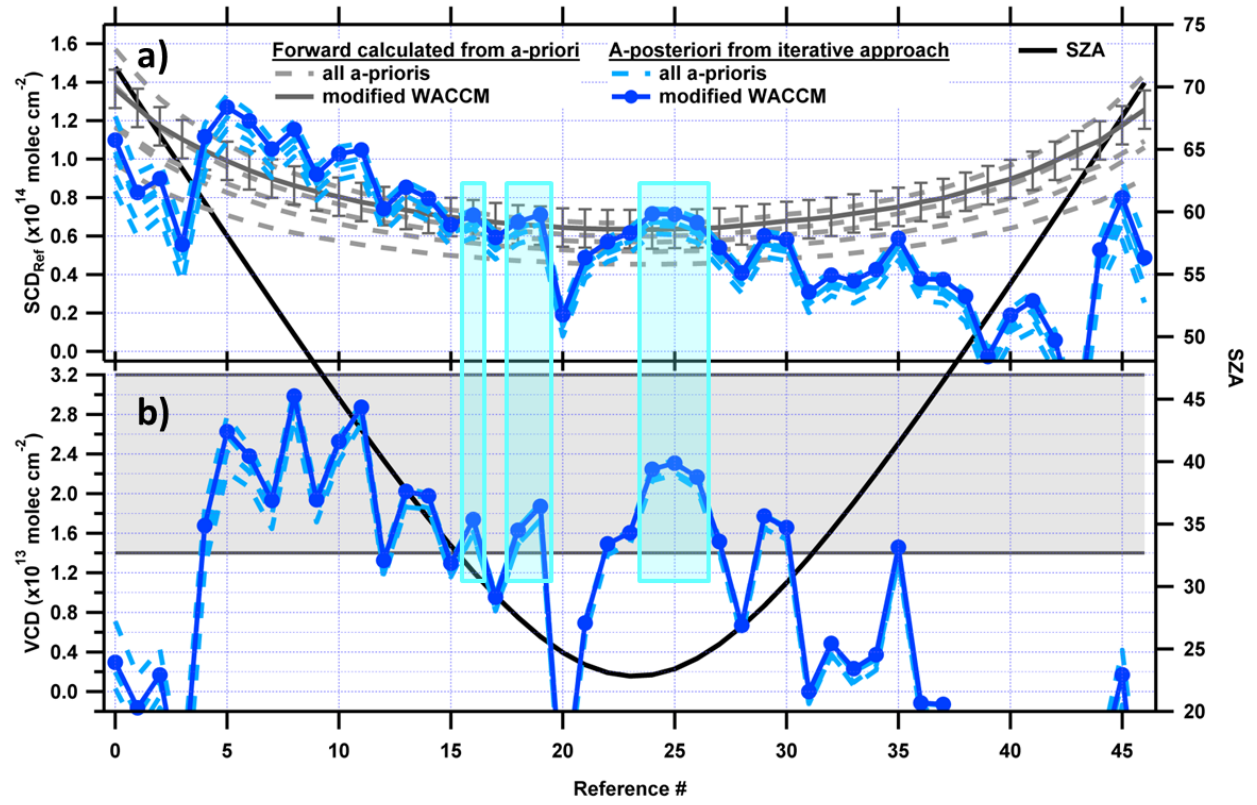


Figure S5

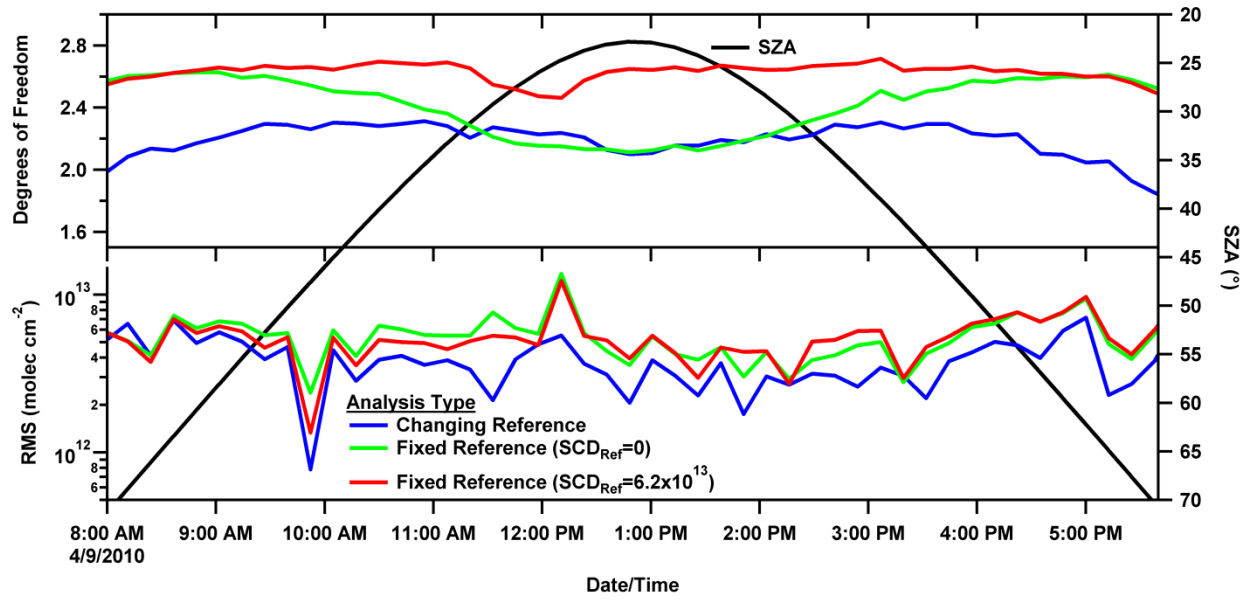


Figure S6

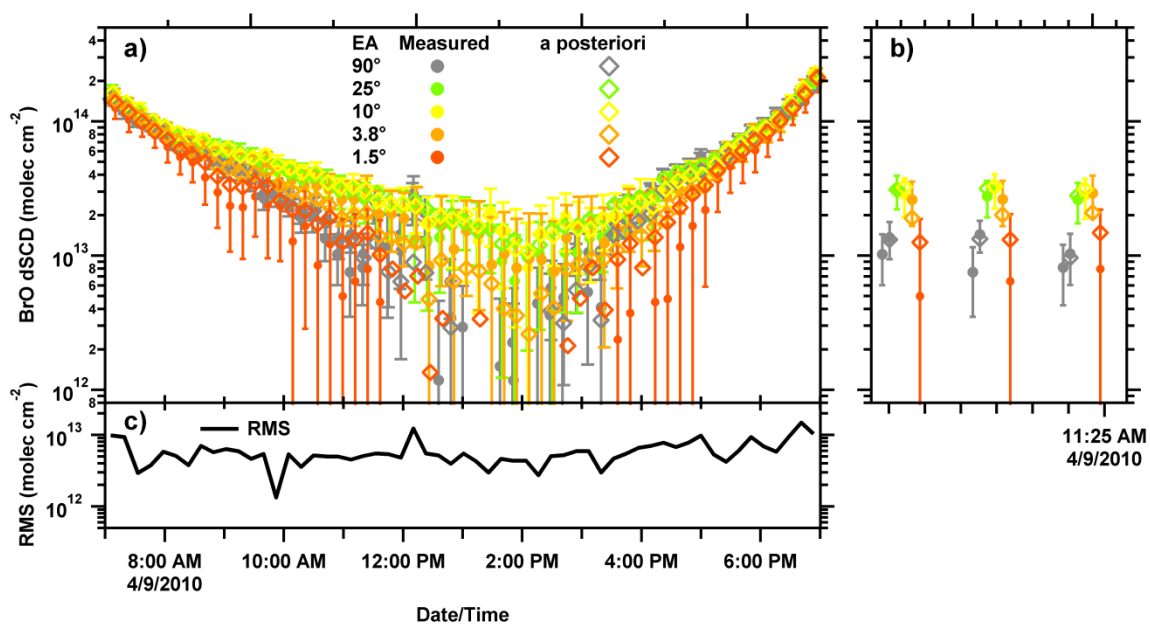


Figure S7

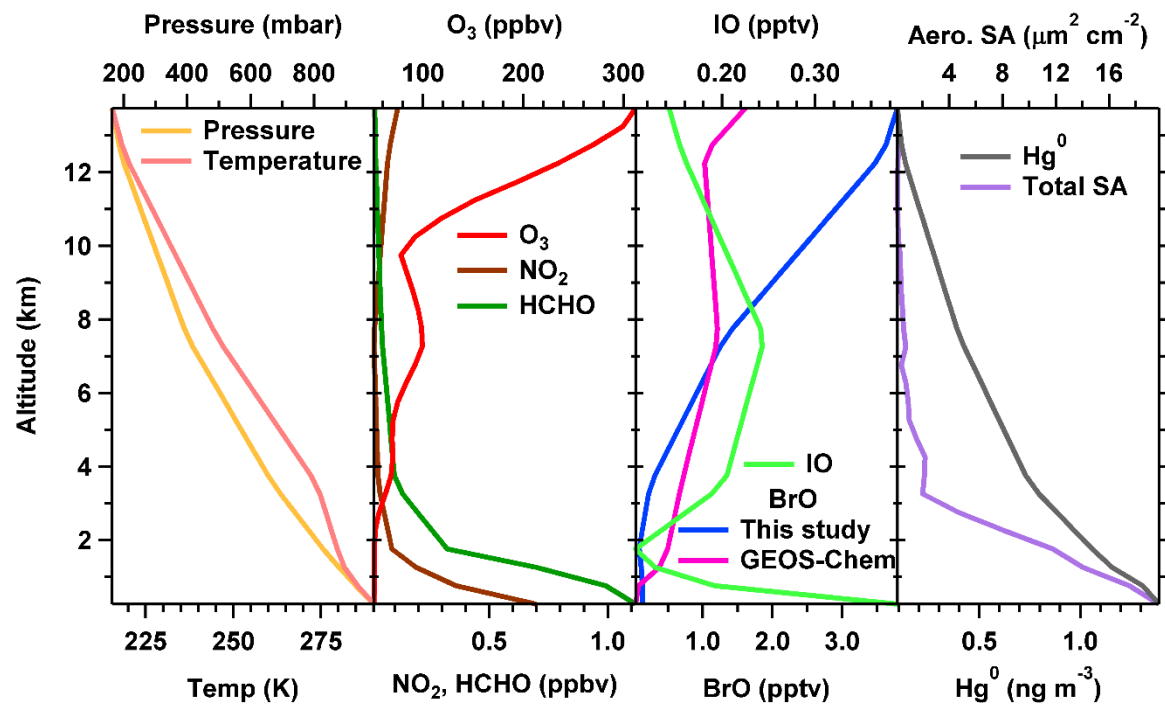


Figure S8

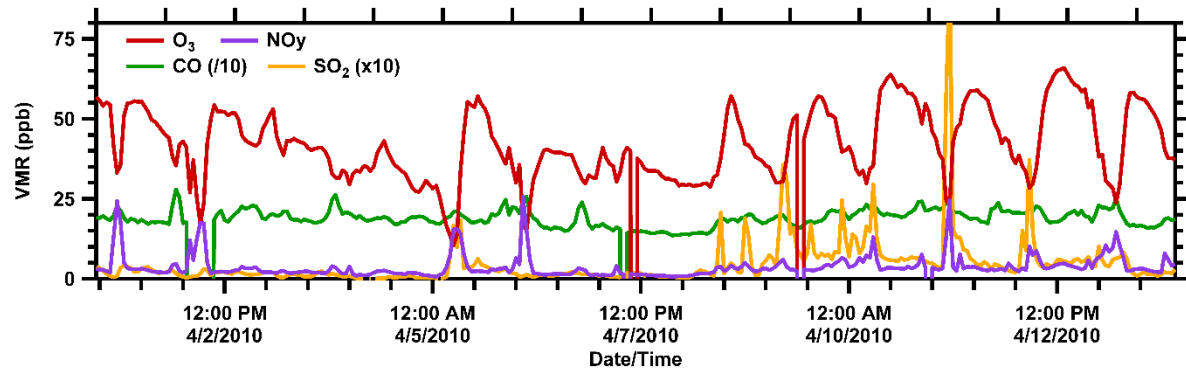


Figure S9

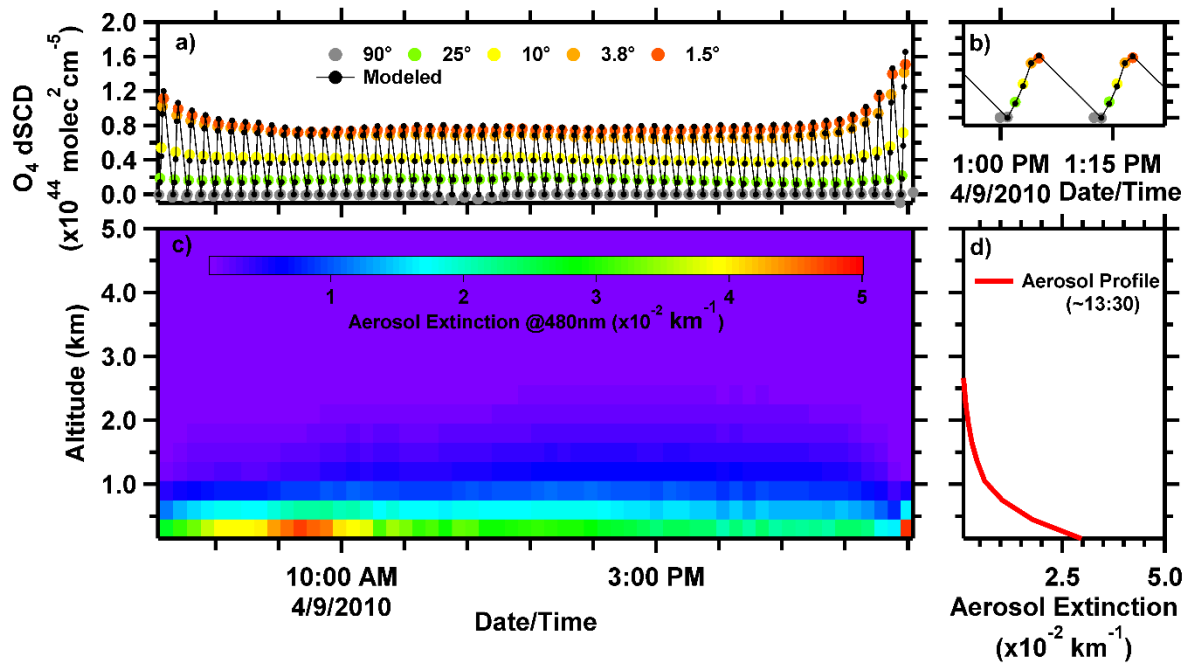


Figure S10

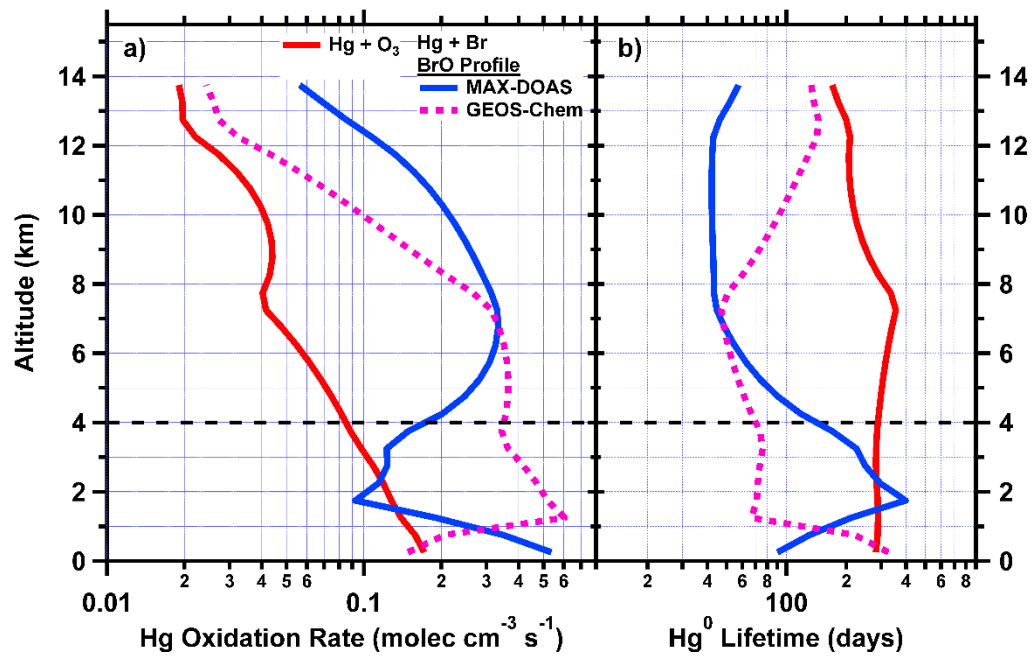


Figure S11